

The Lightest Pseudo-Goldstone Boson at Future e^+e^- Colliders ¹

R. Casalbuoni^{a,b}, A. Deandrea^c, S. De Curtis^b,
D. Dominici^{a,b}, R. Gatto^d and J. F. Gunion^e

^a*Dipartimento di Fisica Università di Firenze, I-50125 Firenze, Italia*

^b*I.N.F.N., Sezione di Firenze, I-50125 Firenze, Italia*

^c*Theoretical Physics Division, CERN, CH-1211 Geneva 23, Switzerland*

^d*Départ. de Physique Théorique, Université de Genève, CH-1211 Genève 4, Suisse*

^e*Department of Physics, University of California, Davis, CA 95616, USA*

Abstract

In a class of models of dynamical symmetry breaking not ruled out by the available data, the lightest neutral pseudo-Nambu-Goldstone boson (P^0) contains only down-type techniquarks and charged technileptons. Its mass scale is naturally determined by the b -quark and therefore it is likely to be light. As the presence of pseudo-Nambu-Goldstone bosons in models of dynamical symmetry breaking is a quite general feature, the search of the P^0 at colliders is an interesting opportunity of putting limits on or discovering a dynamical electroweak symmetry breaking scenario. In this note we discuss the prospects for discovering and studying the P^0 at future e^+e^- and $\gamma\gamma$ colliders.

1 Introduction

The discovery potential of high energy e^+e^- linear colliders and the high-precision with which the properties of particles and their interactions can be analysed have been investigated in a number of studies within the ECFA/DESY Study on Physics and Detectors for a Linear Collider (see [1] and references therein). The linear collider provides also a unique opportunity for the discovery of particles in alternative scenarios, like dynamical symmetry breaking (see for example [2]).

Dynamical symmetry breaking (DSB) avoids the introduction of fundamental scalar fields but generally predicts many pseudo-Nambu-Goldstone bosons (PNGB's) due to the breaking of a large initial global symmetry group G . PNGB's do not acquire mass from the technicolor interactions, therefore they are almost certainly the lightest of the new states in the physical spectrum predicted by DSB. Among the PNGB's, the colorless neutral states are unique in that they remain massless even after the interactions of the color and electroweak gauge bosons are turned on. In technicolor models, their

¹LC-TH-1999-013, proceedings of the Second ECFA/DESY Study on "Physics Studies for a Future Linear Collider", http://www.desy.de/~lcnotes/LCnotes_welcome.html

masses derive entirely from effective four technifermion operators involving two technileptons and two techniquarks. Such operators arise from two sources: the one-loop effective potential generated from the low-energy effective Lagrangian that describes the PNGB's and their interactions with quarks and leptons; and explicit extended-technicolor gauge boson (technileptoquark) exchanges that change a techniquark into a technilepton. The one-loop contributions to the mass-squared matrix for the PNGB's exhibit an underlying $SU(2)_L \times SU(2)_R$ symmetry. The technileptoquark gauge boson exchange contributions automatically preserve this symmetry. When this symmetry is present, the lightest PNGB, denoted P^0 , will contain only down-type techniquarks (and charged technileptons) and, in particular, no up-type techniquarks. As a result, its mass scale is most naturally determined by the b -quark mass and not the t -quark mass. Consequently, it is likely to be much lighter than all the other PNGB's.

Direct observation of a PNGB would not have been possible at any existing accelerator, however light the PNGB's are, unless the number of technicolors, denoted N_{TC} , is very large. Further, indirect constraints, *e.g.* from precision electroweak data, are model-dependent and not particularly robust when the number of technicolors is not large.

In the type of DSB model we consider the P^0 might be the only state that is light enough to be produced at a $\sqrt{s} \leq 500$ GeV first generation e^+e^- collider. The most important production process for the P^0 at an e^+e^- collider is $e^+e^- \rightarrow \gamma P^0$. In the $\gamma\gamma$ collider mode of operation, one searches for $\gamma\gamma \rightarrow P^0$. The $\gamma\gamma P^0$ coupling required in these two cases arises from an anomalous vertex graph and is proportional to N_{TC} , yielding production rates proportional to N_{TC}^2 . For $N_{TC} = 4$, we find that discovery of the P^0 in $e^+e^- \rightarrow \gamma P^0$ will be possible for at least a limited range of masses and that the $\gamma\gamma$ collider will provide very robust P^0 signals allowing for fairly precise measurements of rates in a variety of channels. However, prospects decline at smaller N_{TC} . In order to understand how these results depend upon N_{TC} , we will also consider the minimal, although rather unphysical, reference case of $N_{TC} = 1$.

In the following, the DSB model will be described by a low-energy effective theory. The effective low-energy Lagrangian of the theory contains a Yukawa coupling component that plays two crucial roles. First, it determines the most general form of the couplings of all the PNGB's, in particular those of the P^0 , to SM fermions. Second, the one-loop potential computed from the low-energy effective Yukawa couplings gives contributions to the mass-squared matrix of the PNGB's. The relative size of these one-loop contributions to the mass-squared matrix as compared to the contributions from technileptoquark gauge boson exchange diagrams is model-dependent. However, should the one-loop contributions be dominant, the P^0 mass would then be mostly determined by the same mechanism that is responsible for the quark and lepton masses.

The present theoretical uncertainties associated with DSB models increase the importance of searching for a light P^0 . Discovery of the P^0 , and a study of its properties, would be the first steps in unravelling the underlying DSB theory.

2 P^0 phenomenology

We give a brief summary of the branching fractions and total width of the light P^0 . Details concerning the derivation of these formulas can be found in [3]. A partial list of previous studies concerning PNGB's at e^+e^- colliders is given in [4].

The Yukawa couplings of the light P^0 to fermions are:

$$\mathcal{L}_Y = -i\lambda_b\bar{b}\gamma_5 b P^0 - i\lambda_\tau\bar{\tau}\gamma_5\tau P^0 - i\lambda_\mu\bar{\mu}\gamma_5\mu P^0. \quad (1)$$

In order to explore a representative phenomenological case, we make the parameter choice of refs. [5] and [3]

$$\lambda_b = \sqrt{\frac{2}{3}}\frac{m_b}{v}, \quad \lambda_\tau = -\sqrt{6}\frac{m_\tau}{v}, \quad \lambda_\mu = -\sqrt{6}\frac{m_\mu}{v}. \quad (2)$$

This particular set of couplings is based on the assumption of no relevant cancellations (see [5] for details). More generally, we would have $\lambda_f = \xi_f m_f/v$ with ξ_f a number of the order of 1 which depends on the particular choice of the Yukawa parameters.

The corresponding P^0 mass from the one-loop potential is

$$m_{P^0}^2(\text{one-loop}) = \frac{2\Lambda^2}{\pi^2 v^2} m_b^2 \quad (3)$$

where Λ is a UV cut-off situated in the TeV region and we have neglected contributions to $m_{P^0}^2$ proportional to m_μ^2 and m_τ^2 .

Also of importance are the couplings of the P^0 to a pair of SM gauge bosons arising through the ABJ anomaly. These are model-dependent. We will employ those obtained in the standard technicolor theories of Ref. [6, 7, 8]. The relevant Feynman-rule (which in our notation will include double Wick contractions when two identical gauge bosons are present) for such a coupling can be written in the general form:

$$g_{PV_1 V_2} = \frac{\alpha N_{TC} A_{PV_1 V_2}}{\pi v} \epsilon_{\lambda\mu\nu\rho} p_1^\lambda \epsilon_1^\mu p_2^\nu \epsilon_2^\rho, \quad (4)$$

where for $P = P^0$ we have:

$$A_{P^0\gamma\gamma} = -\frac{4}{\sqrt{6}} \left(\frac{4}{3}\right) \quad (5)$$

$$A_{P^0 Z\gamma} = -\frac{4}{2\sqrt{6}} \left(\frac{1-4s_W^2}{4s_W c_W} - \frac{t_W}{3}\right) \quad (6)$$

$$A_{P^0 ZZ} = -\frac{4}{\sqrt{6}} \left(\frac{1-2s_W^2}{2c_W^2} - \frac{t_W^2}{3}\right) \quad (7)$$

$$A_{P^0 gg} = \frac{1}{\sqrt{6}}, \quad (8)$$

where $s_W = \sin\theta_W$, etc.

In the multi-scale/walking technicolor context the value of v appropriate for determining the P^0 couplings could be smaller than $v = 246$ GeV. From the above explicit formulae, it is apparent that all couplings of interest are proportional to $1/v$, implying that a decrease in v could only increase production rates for the P^0 and, thereby, the ability to discover and study the P^0 .

We will work in the limit in which LQ mass-squared matrix contributions can be neglected relative to the one-loop effective potential contributions of Eq. (3). The magnitude of m_{P^0} in this limit can be better appreciated by writing the one-loop contribution to m_{P^0} from Eq. (3) in the form

$$m_{P^0}(\text{one-loop}) \sim 8 \text{ GeV} \times \Lambda(\text{TeV}). \quad (9)$$

Given that $\Lambda < 10$ TeV is most natural in the model being considered, the P^0 would be likely to have mass below m_Z . Only if Λ is unexpectedly large and/or the LQ contributions are very substantial is it possible that m_{P^0} would be larger than ~ 200 GeV.²

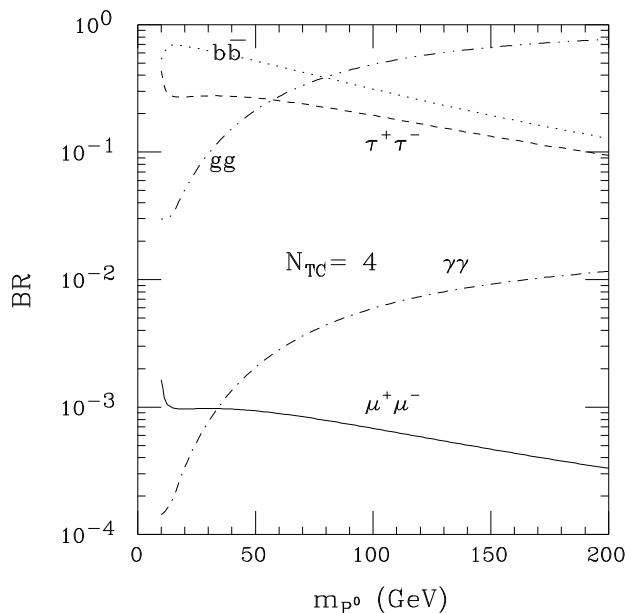


Figure 1: Branching fractions for P^0 decay into $\mu^+\mu^-$, $\tau^+\tau^-$, $b\bar{b}$, $\gamma\gamma$, and gg . We assume $N_{TC} = 4$ and employ the couplings of Eqs. (2), (5) and (8).

The P^0 Yukawa couplings to fermions are given in Eq. (2). For P^0 decays, the $\gamma\gamma$ and gluon-gluon channels are also important; the corresponding couplings are those summarized in Eqs. (5) and (8), as generated by the ABJ anomaly. The corresponding partial widths must be computed keeping in mind that, for our normalization of $A_{P^0\gamma\gamma}$ and A_{P^0gg} , one must include a factor of $1/2$ for identical final state particles:

$$\Gamma(P^0 \rightarrow VV) = \frac{1}{2} C_V \frac{m_{P^0}^3}{32\pi} A_{P^0VV}^2, \quad (10)$$

²Walking/multi-scale technicolor models would have smaller v which would enhance the one-loop contributions to $m_{P^0}^2$ and could also lead to m_{P^0} values above 200 GeV.

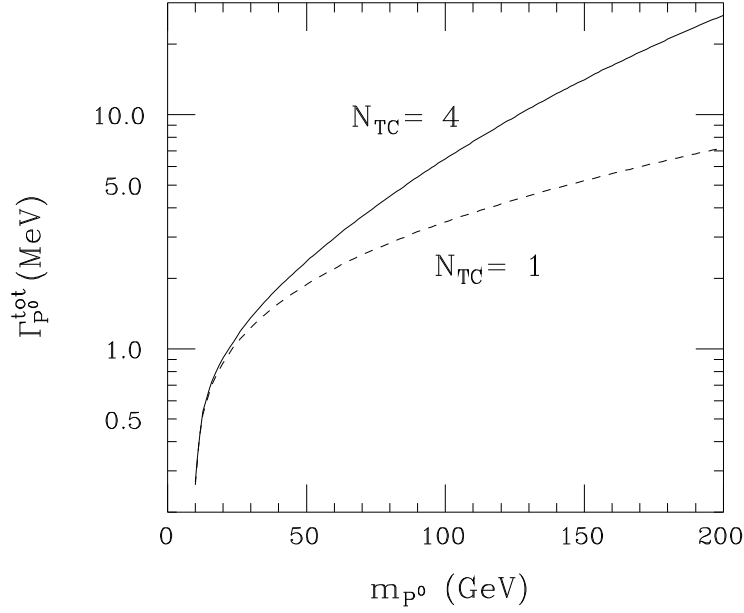


Figure 2: $\Gamma_{P^0}^{\text{tot}}$ as a function of m_{P^0} for $N_{TC} = 4$ and $N_{TC} = 1$. We employ the couplings of Eqs. (2), (5) (8).

where $C_V = 1$ (8) for $V = \gamma$ (g). We list here those partial widths relevant for our analysis:

$$\begin{aligned}
 \Gamma(P^0 \rightarrow \bar{f}f) &= C_F \frac{m_{P^0}}{8\pi} \lambda_f^2 \left(1 - \frac{4m_f^2}{m_{P^0}^2}\right)^{1/2} \\
 \Gamma(P^0 \rightarrow gg) &= \frac{\alpha_s^2}{48\pi^3 v^2} N_{TC}^2 m_{P^0}^3 \\
 \Gamma(P^0 \rightarrow \gamma\gamma) &= \frac{2\alpha^2}{27\pi^3 v^2} N_{TC}^2 m_{P^0}^3, \tag{11}
 \end{aligned}$$

where $C_F = 1(3)$ for leptons (down-type quarks) and N_{TC} is the number of technicolors.

The resulting branching fractions for $N_{TC} = 4$ is shown in Fig. 1, while the total width is shown in Fig. 2. We see that the largest branching fractions are to $b\bar{b}$, $\tau^+\tau^-$ and gg . The total width is typically in the few MeV range, which is similar to that expected for a light SM-like Higgs boson.

There are two important features: first the ratio of $\Gamma(P^0 \rightarrow gg)$ to $\Gamma(h \rightarrow gg)$ is roughly given by $1.5N_{TC}^2$; second the ratio of $B(P^0 \rightarrow \gamma\gamma)$ to $B(h \rightarrow \gamma\gamma)$ is of order 4 for $50 \leq m_{P^0} \leq 150$ GeV if $N_{TC} = 4$, but substantially smaller if $N_{TC} = 1$. If N_{TC} and/or m_{P^0} is large enough that $P^0 \rightarrow gg$ is the dominant decay mode (see Fig. 1), then $B(P^0 \rightarrow \gamma\gamma)$ becomes independent of N_{TC} while $\Gamma(P^0 \rightarrow gg)$ is proportional to N_{TC}^2 , yielding

$$\Gamma(P^0 \rightarrow gg)B(P^0 \rightarrow \gamma\gamma) \rightarrow \frac{2\alpha^2}{27\pi^3} \frac{N_{TC}^2 m_{P^0}^3}{v^2} \sim 2.4 \times 10^{-3} \text{ MeV } N_{TC}^2 \left(\frac{m_{P^0}}{100 \text{ GeV}}\right)^3, \tag{12}$$

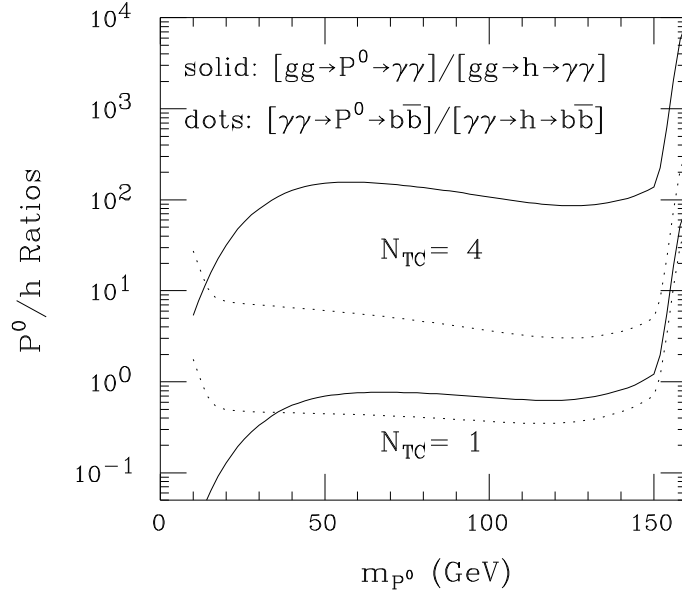


Figure 3: The ratios $[\Gamma(P^0 \rightarrow gg)B(P^0 \rightarrow \gamma\gamma)]/[\Gamma(h \rightarrow gg)B(h \rightarrow \gamma\gamma)]$ (solid curves) and $[\Gamma(P^0 \rightarrow \gamma\gamma)B(P^0 \rightarrow b\bar{b})]/[\Gamma(h \rightarrow \gamma\gamma)B(h \rightarrow b\bar{b})]$ (dotted curves), where h is the SM Higgs boson, are plotted as a function of m_{P^0} , taking $m_h = m_{P^0}$. Results are given for $N_{TC} = 4$ and $N_{TC} = 1$ using the specific P^0 couplings of Eqs. (2), (5) and (8).

which, for $N_{TC} = 4$, is typically much larger than the corresponding result for a SM-like Higgs boson. This will make P^0 discovery in the $\gamma\gamma$ final state at a hadron collider much easier than in the SM Higgs case when $N_{TC} = 4$. Similarly, for $N_{TC} = 4$, one finds a larger value of $\Gamma(P^0 \rightarrow \gamma\gamma)B(P^0 \rightarrow b\bar{b})$ as compared to the SM h analogue. This implies that discovery of the P^0 in $\gamma\gamma$ collisions will be much easier than for a SM Higgs boson. Of course, both ratios are smaller for smaller N_{TC} . In the minimal $N_{TC} = 1$ case, these two ratios are both of order 0.4 to 0.9 for $30 \leq m_{P^0} \leq 150$ GeV, implying that the ability to detect the P^0 would be about the same as for the SM Higgs boson over this mass range.

3 P^0 production at e^+e^- colliders

First, let us consider whether LEP places any limits on the P^0 . At LEP the dominant production mode is $Z \rightarrow \gamma P^0$. The width for this decay is given by

$$\Gamma(Z \rightarrow \gamma P^0) = \frac{\alpha^2 m_Z^3}{96\pi^3 v^2} N_{TC}^2 A_{P^0 Z \gamma}^2 \left(1 - \frac{m_{P^0}^2}{m_Z^2}\right)^3, \quad (13)$$

where $A_{P^0 Z \gamma}$ appeared in Eq. (6). Let us follow Ref. [9] and require that the $Z \rightarrow \gamma P^0$ decay width be $> 2 \times 10^{-6}$ GeV in order for the P^0 to be visible in a sample of 10^7 Z bosons. We see that $N_{TC} \gtrsim 8$ is required at $m_{P^0} = 0$, rising rapidly as m_{P^0} increases.³

³In a multi-scale model, where the effective v could be smaller, these results would be altered.

We now consider LEP2. The general form of the cross section for PV production (from Ref. [10]) is

$$\begin{aligned} \sigma(e^+e^- \rightarrow PV) &= \frac{\alpha^3 N_{TC}^2}{24\pi^2 v^2} \lambda^{3/2}(1, m_P^2/s, m_V^2/s) \\ &\times \left[A_{PV\gamma}^2 + \frac{A_{PV\gamma} A_{PVZ}(1 - 4s_W^2)}{2c_W s_W (1 - m_Z^2/s)} + \frac{A_{PVZ}^2(1 - 4s_W^2 + 8s_W^4)}{8c_W^2 s_W^2 (1 - m_Z^2/s)^2} \right], \end{aligned} \quad (14)$$

where $V = \gamma, Z$ and P is the PNCB. In the above, we have neglected the Z width. As already stated, the best mode for P^0 production at an e^+e^- collider (with $\sqrt{s} > m_Z$) is $e^+e^- \rightarrow \gamma P^0$. Because the $P^0 Z \gamma$ coupling-squared is much smaller than the $P^0 \gamma \gamma$ coupling-squared (by a factor of nearly 400), the dominant diagram is $e^+e^- \rightarrow \gamma \rightarrow \gamma P^0$, proportional to $A_{P^0\gamma\gamma}^2$. Even when kinematically allowed, rates in the $e^+e^- \rightarrow Z P^0$ channel are substantially smaller, as we shall discuss. We will give results for the moderate value of $N_{TC} = 4$. For $\sqrt{s} = 200$ GeV, we find that, after imposing an angular cut of $20^\circ \leq \theta \leq 160^\circ$ on the outgoing photon (a convenient acceptance cut that also avoids the forward/backward cross section singularities but is more than 91% efficient), the $e^+e^- \rightarrow \gamma P^0$ cross section is below 1 fb for $N_{TC} = 4$. Given that the maximum integrated luminosity anticipated is of order $L \sim 0.5 \text{ fb}^{-1}$, we conclude that LEP2 will not allow detection of the P^0 unless N_{TC} is very large.

The cross section for $e^+e^- \rightarrow \gamma P^0$ at $\sqrt{s} = 500$ GeV, after imposing the same angular cut as for LEP2, is illustrated in Fig. 4 for $N_{TC} = 4$. It ranges from 0.9 fb down to 0.5 fb as m_{P^0} goes from zero up to ~ 200 GeV. For $L = 50 \text{ fb}^{-1}$, we have at most 45 events with which to discover and study the P^0 . The $e^+e^- \rightarrow Z P^0$ cross section is even smaller. Without cuts and without considering any specific Z or P^0 decay modes, it ranges from 0.014 fb down to 0.008 fb over the same mass range. If TESLA is able to achieve $L = 500 \text{ fb}^{-1}$ per year, γP^0 production will have a substantial rate, but the $Z P^0$ production rate will still not be useful. Since the γP^0 production rate scales as N_{TC}^2 , if $N_{TC} = 1$ a $\sqrt{s} = 500$ GeV machine will yield at most 3 (30) events for $L = 50 \text{ fb}^{-1}$ (500 fb^{-1}), making P^0 detection and study extremely difficult. Thus, we will focus our analysis on the $N_{TC} = 4$ case.

In order to assess the γP^0 situation more fully, we must consider backgrounds. As we have seen, the dominant decay of the P^0 is typically to $b\bar{b}$, $\tau^+\tau^-$ or gg . For the $b\bar{b}$ and gg modes, the backgrounds relevant to the γP^0 channel are $\gamma b\bar{b}$, $\gamma c\bar{c}$ and $\gamma q\bar{q}$ ($q = u, d, s$) production. The cross sections for these processes obtained after integrating over a 10 GeV bin size in the quark-antiquark mass (an optimistic estimate of the resolution that could be achieved using reconstruction of the quark-antiquark or $\tau^+\tau^-$ pair) are also given in Fig. 4. For $10 \lesssim m_{P^0} \lesssim 80$ GeV and $m_{P^0} \geq 100$ GeV, the signal to background ratio is not too much smaller than 1. We will assess the P^0 discovery potential in specific channels by assuming that 10 GeV mass resolution can be achieved for m_{P^0} in each case.

In order to proceed with a discussion of specific final states, we state our assumptions regarding tagging and mis-tagging efficiencies. We separate $\tau^+\tau^-$, $b\bar{b}$, $c\bar{c}$ and $q\bar{q}/gg$ final states by using topological and τ tagging with efficiencies and mis-tagging probabilities as estimated by B. King [11] for the muon collider. These are slightly pessimistic for an

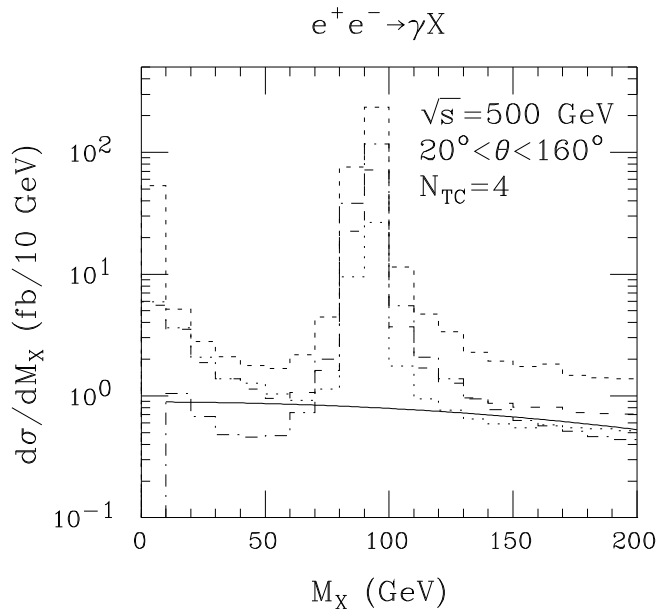


Figure 4: Taking $N_{TC} = 4$, the cross section (in fb) for $e^+e^- \rightarrow \gamma P^0$ (solid curve) is plotted as a function of m_{P^0} in comparison to various possible backgrounds: $e^+e^- \rightarrow \gamma b\bar{b}$ (dotdash); $e^+e^- \rightarrow \gamma c\bar{c}$ (dashes); $e^+e^- \rightarrow \gamma q\bar{q}$, $q = u, d, s$ (small dashes); and $e^+e^- \rightarrow \gamma \tau^+\tau^-$ (dots). The background cross sections are integrated over a $\Delta M_X = 10$ GeV bin width (a possible approximation to the resolution that can be achieved). A cut of $20^\circ \leq \theta \leq 160^\circ$ has been applied to both the signal and the backgrounds. Effects due to tagging and mis-tagging are discussed in the text.

e^+e^- collider. We take $\epsilon_{bb} = 0.55$, $\epsilon_{cc} = 0.38$, $\epsilon_{bc} = 0.18$, $\epsilon_{cb} = 0.03$, $\epsilon_{qb} = \epsilon_{gb} = 0.03$, $\epsilon_{qc} = \epsilon_{gc} = 0.32$, $\epsilon_{\tau\tau} = 0.8$, $\epsilon_{\tau b} = \epsilon_{\tau c} = \epsilon_{\tau q} = 0$, where the notation is that ϵ_{ab} is the probability that a particle/jet of type a is tagged as being of type b . Gluons are treated the same as light quarks.

Results for S/\sqrt{B} , in the various tagged channels, for $N_{TC} = 4$ and assuming $L = 100 \text{ fb}^{-1}$ at $\sqrt{s} = 500 \text{ GeV}$, are plotted in Fig. 5. We have assumed a mass window of $\Delta M_X = 10 \text{ GeV}$ in evaluating the backgrounds in the various channels. Also shown in Fig. 5 is the largest S/\sqrt{B} that can be achieved by considering (at each m_{P^0}) all possible combinations of the gg , $c\bar{c}$, $b\bar{b}$ and $\tau^+\tau^-$ channels. From the figure, we find $S/\sqrt{B} \geq 3$ (our discovery criterion) for $m_{P^0} \leq 75 \text{ GeV}$ and $m_{P^0} \geq 130 \text{ GeV}$, *i.e.* outside the Z region. A strong signal, $S/\sqrt{B} \sim 4$, is only possible for $m_{P^0} \sim 20 - 60 \text{ GeV}$. As the figure shows, the signal in any one channel is often too weak for discovery, and it is only the best channel combination that will reveal a signal. For the TESLA $L = 500 \text{ fb}^{-1}$ luminosity, S/\sqrt{B} should be multiplied by ~ 2.2 and discovery prospects will be improved.

Once a PNGB is discovered, one will wish to determine the branching fractions and couplings as precisely as possible in order to pin down the fundamental parameters of the model. In the $e^+e^- \rightarrow \gamma P^0$ production mode, one will begin by extracting ratios of branching fractions by computing ratios of the rates measured in various final state

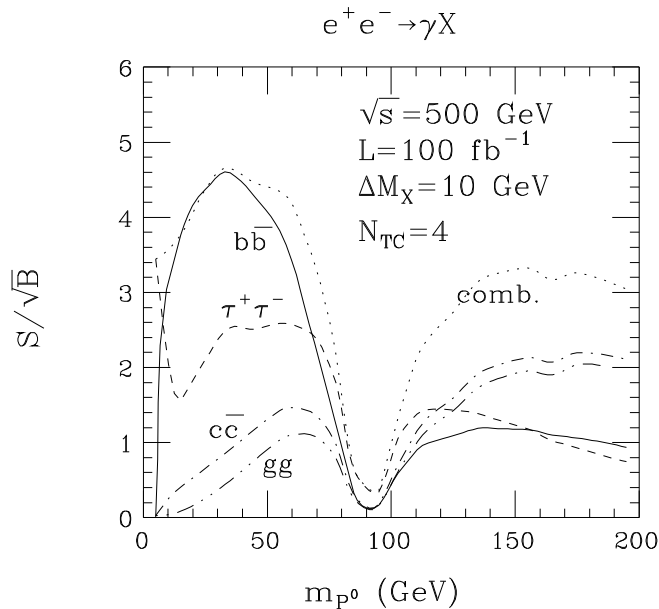


Figure 5: We consider $e^+e^- \rightarrow \gamma X$ taking $N_{TC} = 4$ and, for $L = 100 \text{ fb}^{-1}$ at $\sqrt{s} = 500 \text{ GeV}$, plot the statistical significances S/\sqrt{B} for a P^0 signal in various ‘tagged’ channels as a function of m_{P^0} . We assume mass resolution of $\Delta M_X = 10 \text{ GeV}$ in each channel and the channel tagging and mis-tagging probabilities discussed in the text. A cut of $20^\circ \leq \theta \leq 160^\circ$ has been imposed on both the signal and the backgrounds. The curve legend is: gg (dot-dot-dash); $c\bar{c}$ (dot-dash); $b\bar{b}$ (solid); $\tau^+\tau^-$ (dashes). Also shown (dots) is the largest S/\sqrt{B} that can be achieved by considering all possible combinations of channels.

channels.⁴ As a first indication of how well one can do, we give, in Fig. 6, the statistical errors $(S+B)^{1/2}/S$ in each of the tagged channels in the case of our bench mark example of the P^0 . Even if we decrease the errors of the figure by the $\sqrt{5} \sim 2.2$ factor appropriate for an integrated luminosity of $L = 500 \text{ fb}^{-1}$, the only channel with reasonable error ($\lesssim 15\%$) would be $b\bar{b}$. Further, in obtaining results for ratios of $B(P^0 \rightarrow F)$ for $F = gg, b\bar{b}, \tau^+\tau^-$, one must unfold the mis-tagging (implying introduction of systematic uncertainties) and combine statistical errors in the various tagged channels.

The next step, beyond the extraction of ratios of the P^0 branching fractions, is the model-independent determination of the individual $B(P^0 \rightarrow F)$ ’s for specific final states F via the ratio of the rate in a specific final state to the inclusive rate:

$$B(P^0 \rightarrow F) = \frac{\sigma(e^+e^- \rightarrow \gamma P^0)B(P^0 \rightarrow F)}{\sigma(e^+e^- \rightarrow \gamma P^0)}. \quad (15)$$

The crucial issue is then the ability to observe the P^0 inclusively in the γX final state as a peak in the recoil M_X spectrum, and the associated error in the inclusive cross

⁴Note that the reason we focus on ratios is that the systematic errors due to uncertainty in the absolute normalization of the rate in any given channel will cancel out in the ratios.

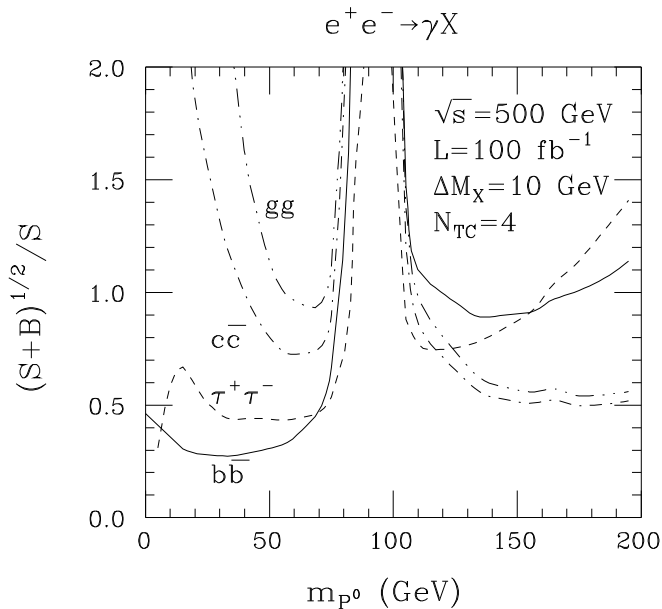


Figure 6: We consider $e^+e^- \rightarrow \gamma P^0 \rightarrow \gamma X$ production for $N_{TC} = 4$, with $L = 100 \text{ fb}^{-1}$ at $\sqrt{s} = 500 \text{ GeV}$, and plot the statistical error $(S+B)^{1/2}/S$ for the various ‘tagged’ channel rates ($X = \tau^+\tau^-$, $b\bar{b}$, $c\bar{c}$, $g\bar{g}$) as a function of m_{P^0} . Assumptions and notation as in Fig. 5.

section $\sigma(e^+e^- \rightarrow \gamma P^0)$. The resolution in M_X is determined by the photon energy resolution. Using $\Delta E_\gamma/E_\gamma = 0.12/\sqrt{E_\gamma} \oplus 0.01$, one finds $\pm 1\sigma$ mass windows in m_{P^0} of $[0, 78]$, $[83.5, 114]$ and $[193, 207]$ (GeV units) for $m_{P^0} = 55$, 100 and 200 GeV, respectively. If the resolution could be improved to $\Delta E_\gamma/E_\gamma = 0.08/\sqrt{E_\gamma} \oplus 0.005$ [12], then the mass windows for $m_{P^0} = 55$, 100 and 200 GeV become $[36, 69]$, $[91, 108]$ and $[196, 204]$, respectively. [We note that $\Delta E_\gamma/E_\gamma \gtrsim 0.0125$ ($\gtrsim 0.0075$) for $m_{P^0} \leq 200$ GeV for the first (second) resolution case, indicating that the constant term is dominant and should be the focus for improving this particular signal.]

Backgrounds to inclusive γP^0 detection will be substantial. All the backgrounds plotted in Fig. 4 must be included (integrated over the appropriate mass window), and others as well. Observation of the P^0 signal in the recoil M_X spectrum would be difficult, especially for lower values of m_{P^0} . However, if m_{P^0} is known ahead of time, then one can simply employ the appropriate mass window and estimate the background from M_X bins outside the mass window. We anticipate that the resulting errors for $\sigma(e^+e^- \rightarrow \gamma P^0)$ will be large, implying that the corresponding model-independent determinations of the various $B(P^0 \rightarrow F)$ ’s from Eq. (15) will be subject to large statistical uncertainty. This is an important loss relative to the usual program for determining the properties of a Higgs boson in a model-independent manner using the $e^+e^- \rightarrow Zh$ signal in the inclusive $e^+e^- \rightarrow ZX$ final state.

4 P^0 production at a $\gamma\gamma$ collider

The rate for production and decay of a narrow resonance R in $\gamma\gamma$ collisions is given by [13]

$$N(\gamma\gamma \rightarrow R \rightarrow F) = \frac{8\pi\Gamma(R \rightarrow \gamma\gamma)B(R \rightarrow F)}{m_R^2 E_{e^+e^-}} \tan^{-1} \frac{\Gamma_{\text{exp}}}{\Gamma_R^{\text{tot}}} (1 + \langle\lambda\lambda'\rangle) G(y_R) L_{e^+e^-}, \quad (16)$$

where λ and λ' are the helicities of the colliding photons, Γ_{exp} is the mass interval accepted in the final state F and $L_{e^+e^-}$ is the integrated luminosity for the colliding electron and positron beams. In Eq. (16), $\langle\lambda\lambda'\rangle$ and $G(y_R \equiv m_R/E_{e^+e^-})$ depend upon the details of the $\gamma\gamma$ collision set-up. Here, we are interested in exploring the ability of a $\gamma\gamma$ collider to discover the narrow P^0 resonance and so we choose laser polarizations P and P' and e^+e^- beam helicities λ_e and λ'_e in the configuration $2\lambda_e P \sim +1$, $2\lambda'_e P' \sim +1$, $PP' \sim +1$ such that $G \gtrsim 1$ and $\langle\lambda\lambda'\rangle \sim 1$ (which suppresses $\gamma\gamma \rightarrow q\bar{q}$ backgrounds) over the large range $0.1 \leq y_R \leq 0.7$. The P^0 is always sufficiently narrow that $\tan^{-1} \rightarrow \pi/2$. In this limit, the rate is proportional to $\Gamma(R \rightarrow \gamma\gamma)B(R \rightarrow F)$. For the P^0 , $\Gamma(P^0 \rightarrow \gamma\gamma)$ is large and the total production rate will be substantial. In this regard, the importance of the eigenstate composition of the P^0 has already been noted; *e.g.* for the same mass, if the π_D were the mass eigenstate it would have only 1/8 the production rate.

In Fig. 3, we plotted $\Gamma(P^0 \rightarrow \gamma\gamma)B(P^0 \rightarrow b\bar{b})$ divided by $\Gamma(h \rightarrow \gamma\gamma)B(h \rightarrow b\bar{b})$, where h denotes the SM Higgs boson, for both $N_{TC} = 4$ and $N_{TC} = 1$. Over the $m_{P^0} = m_h$ range from 15 to 150 GeV, the ratio for $N_{TC} = 4$ varies from ~ 8 down to ~ 3 , rising to very large values at masses above 160 GeV where the $h \rightarrow WW, ZZ$ decay modes open up. For $N_{TC} = 1$, this same ratio is order 0.4 to 0.5 over the 15 to 150 GeV mass range, again rising dramatically at higher masses. Since it is well-established [13, 14, 15] that the SM h can be discovered in this decay mode for $40 \lesssim m_h \lesssim 2m_W$, it is clear that P^0 discovery in the $b\bar{b}$ final state will be possible up to at least 200 GeV, down to $\sim 0.1\sqrt{s} \sim 50$ GeV (at $\sqrt{s} \sim 500$ GeV), below which $G(y)$ starts to get small. Discovery at lower values of m_{P^0} would require lowering the \sqrt{s} of the machine.

In order to quantify these claims slightly further, we have taken the results of Ref. [13] (Fig. 2) for the SM Higgs $b\bar{b}$ signal and the $b\bar{b}$ background rate and multiplied the former by the $\Gamma(\gamma\gamma)B(b\bar{b})$ ratio plotted in Fig. 3 and by the correction factor

$$\tan^{-1}(\Gamma_{\text{exp}}/\Gamma_{P^0}^{\text{tot}})/\tan^{-1}(\Gamma_{\text{exp}}/\Gamma_h^{\text{tot}}) \quad (17)$$

[see Eq. (16)]. The resulting signal and background rates are plotted for $N_{TC} = 4$ in Fig. 7, assuming that $L_{\text{eff}} \equiv G(y_{P^0})L_{e^+e^-} = 20 \text{ fb}^{-1}$, independent of m_{P^0} . (As already stated, to achieve $G \gtrsim 1$ at the lowest masses would require lowering the machine energy so that $m_{P^0}/\sqrt{s} > 0.1 - 0.2$.) For the $b\bar{b}$ channel S/\sqrt{B} is plotted in Fig. 8.

We have also performed this same study for $N_{TC} = 1$. The signal rate is, of course, significantly reduced relative to $N_{TC} = 4$ by virtue of the large decrease in $\Gamma(P^0 \rightarrow \gamma\gamma)$. As Fig. 3 shows, we expect rates similar to those for a SM Higgs; in the $b\bar{b}$ final state, S ranges from 40 up to 170 as m_{P^0} goes from 20 to 200 GeV. The corresponding S/\sqrt{B}

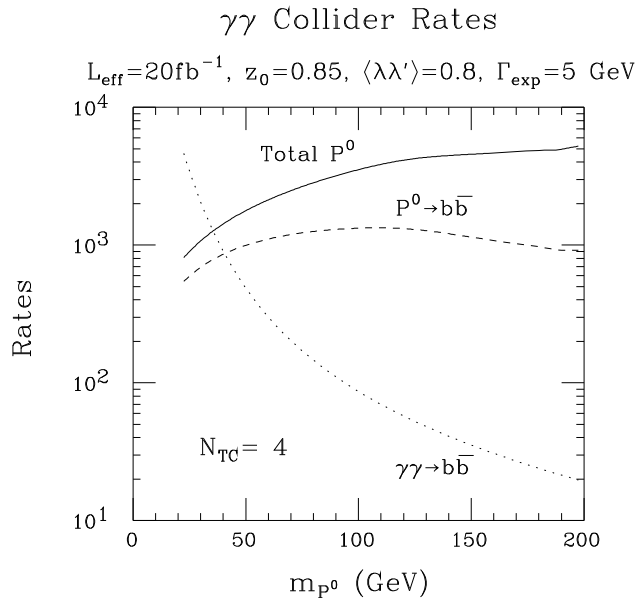


Figure 7: We consider $\gamma\gamma$ collisions for $L_{\text{eff}} = 20 \text{ fb}^{-1}$ (assumed independent of m_{P^0}), with an angular cut of $|\cos\theta| < 0.85$ applied to the two-particle final state. An experimental resolution $\Gamma_{\text{exp}} = 5$ GeV is assumed in the final state. We plot, as a function of m_{P^0} : the total $\gamma\gamma \rightarrow P^0$ production rate (solid); the rate for $\gamma\gamma \rightarrow P^0 \rightarrow b\bar{b}$ (dashes); and the $\gamma\gamma \rightarrow b\bar{b}$ irreducible background rate (dots). $N_{TC} = 4$ is assumed.

values are plotted in Fig. 8. For $m_{P^0} > 60$ GeV, there is an excellent chance that P^0 detection will be possible in $\gamma\gamma$ collisions even for the minimal $N_{TC} = 1$ choice.

Of course, these results are not entirely realistic. The $\gamma\gamma \rightarrow b\bar{b}$ background rate plotted assumes an unrealistically small $b\bar{b}$ mass resolution of $\Gamma_{\text{exp}} = 5$ GeV. In addition, backgrounds from $\gamma\gamma \rightarrow c\bar{c}g$ and $\gamma\gamma \rightarrow b\bar{b}g$ are ignored. (These are not suppressed by having $\langle\lambda\lambda'\rangle \sim 1$.) However, these three-jet backgrounds can be largely eliminated by using topological tagging and cuts designed to isolate the two-jet final state. The resulting additional efficiency reduction for the $P^0 \rightarrow b\bar{b}$ signal is typically no smaller than $\gtrsim 0.5$ (for single- b topological tagging) [15]. Thus, P^0 discovery at a $\gamma\gamma$ collider in the $b\bar{b}$ final state will be very viable over a large mass range.

Once the P^0 has been discovered, either in $\gamma\gamma$ collisions or elsewhere, one can configure the $\gamma\gamma$ collision set-up so that the luminosity is peaked at $\sqrt{s}_{\gamma\gamma} \sim m_{P^0}$. A very precise measurement of the P^0 rate in the $b\bar{b}$ final state will then be possible if $N_{TC} = 4$. For example, rescaling the SM Higgs ‘single-tag’ results of Table 1 of Ref. [15] (which assumes a peaked luminosity distribution with a total of $L = 10 \text{ fb}^{-1}$) for the $106 \text{ GeV} \leq m_{jj} \leq 126 \text{ GeV}$ mass window to the case of the P^0 using the $[\Gamma(P^0 \rightarrow \gamma\gamma)B(P^0 \rightarrow b\bar{b})]/[\Gamma(h \rightarrow \gamma\gamma)B(h \rightarrow b\bar{b})]$ ratio for $N_{TC} = 4$, plotted in Fig. 3, we obtain $S \sim 5640$ compared to $B \sim 325$, after angular, topological tagging and jet cuts. This implies a statistical error for measuring $\Gamma(P^0 \rightarrow \gamma\gamma)B(P^0 \rightarrow b\bar{b})$ of $\lesssim 1.5\%$. Systematic errors will probably dominate. Following the same procedure for $N_{TC} = 1$, we find (at this mass) a statistical

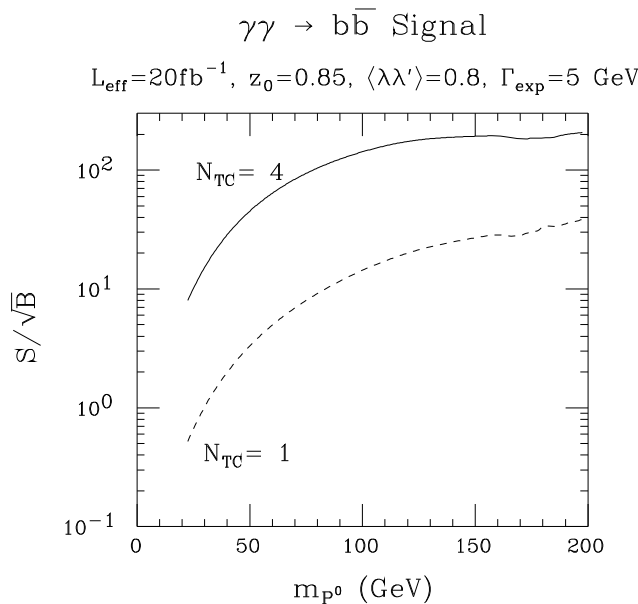


Figure 8: We consider $\gamma\gamma$ collisions for $L_{\text{eff}} = 20 \text{ fb}^{-1}$ (assumed independent of m_{P^0}), with an angular cut of $|\cos\theta| < 0.85$ applied to the two-particle final state. An experimental resolution $\Gamma_{\text{exp}} = 5 \text{ GeV}$ is assumed in the final state. We plot, as a function of m_{P^0} , the statistical significance S/\sqrt{B} for $N_{TC} = 4$ and $N_{TC} = 1$.

error for this measurement of $\lesssim 5\%$. Of course, for lower masses the error will worsen. For $N_{TC} = 4$, we estimate an error for the $b\bar{b}$ rate measurement still below 10% even at a mass as low as $m_{P^0} = 20 \text{ GeV}$ (assuming the \sqrt{s} of the machine is lowered sufficiently to focus on this mass without sacrificing luminosity). For $N_{TC} = 1$, we estimate an error for the $b\bar{b}$ rate measurement of order 15 – 20% for $m_{P^0} \sim 60 \text{ GeV}$.

Of course, it would be very interesting to measure rates in other final state channels as well. The $N_{TC} = 4$ total P^0 rate shown in Fig. 7 (which can be further increased once m_{P^0} is known and the $\gamma\gamma$ collisions are configured for a peaked, rather than broad, luminosity spectrum) indicates that $\gamma\gamma \rightarrow P^0 \rightarrow \tau^+\tau^-$ and gg will also have large event rates. Backgrounds are probably too large in the gg final state to obtain a robust P^0 signal. Backgrounds in the $\tau^+\tau^-$ channel are not a large, but there is no sharp mass peak in this channel. Still, if one configures the machine energy and $\gamma\gamma$ collision set-up so that the $\gamma\gamma$ luminosity is very peaked at an already known value of m_{P^0} , a reasonably precise measurement of $\Gamma(P^0 \rightarrow \gamma\gamma)B(P^0 \rightarrow \tau^+\tau^-)$ might prove possible. Detailed studies of what can be achieved in the gg and $\tau^+\tau^-$ channels should be performed.

For $N_{TC} = 4$, it might even be possible to detect the P^0 in the $\gamma\gamma \rightarrow P^0 \rightarrow \gamma\gamma$ mode. The (broad-luminosity-profile) total P^0 production rate plotted in Fig. 7 is > 3500 for $m_{P^0} > 100 \text{ GeV}$, for which masses $B(P^0 \rightarrow \gamma\gamma) > 0.006$ (Fig. 1). The resulting total $\gamma\gamma \rightarrow P^0 \rightarrow \gamma\gamma$ event rate ranges from a low of ~ 20 at $m_{P^0} \sim 100 \text{ GeV}$ to ~ 50 at $m_{P^0} \sim 200 \text{ GeV}$. These rates can be substantially increased if the $\gamma\gamma$ collision set-up is optimized for a known value of m_{P^0} . Presumably the (one-loop) irreducible

$\gamma\gamma \rightarrow \gamma\gamma$ background is quite small. But, one must worry about jets that fake photons and possibly about back-scattered photons that simply pass through into the final state without interacting. (Presumably a minimum-angle cut could be used to largely eliminate the latter.) Once again, a detailed study will be needed to reliably assess prospects for detection of the $P^0 \rightarrow \gamma\gamma$ signal.

5 Conclusion

We have discussed the production of the lightest pseudo-Nambu Goldstone state of a typical technicolor model at future e^+e^- and $\gamma\gamma$ colliders. In the class of models considered, the P^0 is of particular interest because it contains only down-type techniquarks (and charged technileptons) and thus will have a mass scale that is most naturally set by the mass of the b -quark.

We have considered a m_{P^0} mass range that is typically suggested by technicolor models, $10 \text{ GeV} < m_{P^0} < 200 \text{ GeV}$. An e^+e^- collider, while able to discover the P^0 via $e^+e^- \rightarrow \gamma P^0$, so long as m_{P^0} is not close to m_Z and $N_{TC} \geq 3$, is unlikely (unless the TESLA 500 fb^{-1} per year option is built or N_{TC} is very large) to be able to determine the rates for individual γF final states ($F = b\bar{b}, \tau^+\tau^-, gg$ being the dominant P^0 decay modes) with sufficient accuracy.

The $\gamma\gamma$ collider option at an e^+e^- collider is actually a more robust means for discovering the P^0 than direct operation in the e^+e^- collision mode. For $N_{TC} = 4$, we find that $\gamma\gamma \rightarrow P^0 \rightarrow b\bar{b}$ should yield an easily detectable P^0 signal for $0.1 \lesssim \frac{m_{P^0}}{\sqrt{s}} \lesssim 0.7$ when the $\gamma\gamma$ collision set-up is chosen to yield a broad luminosity distribution. Once m_{P^0} is known, the $\gamma\gamma$ collision set-up can be re-configured to yield a luminosity distribution that is strongly peaked at $\sqrt{s}_{\gamma\gamma} \sim m_{P^0}$ and, for much of the mass range of $m_{P^0} \lesssim 200 \text{ GeV}$, a measurement of $\Gamma(P^0 \rightarrow \gamma\gamma)B(P^0 \rightarrow b\bar{b})$ can be made with statistical accuracy in the $\lesssim 2\%$ range. For $N_{TC} = 1$, P^0 discovery in the $\gamma\gamma \rightarrow P^0 \rightarrow b\bar{b}$ channel will remain possible for $m_{P^0} \geq 60 \text{ GeV}$ or so, but the accuracy with which the rate will eventually be measured worsens to $5 - 10\%$.

References

- [1] ECFA/DESY LC Physics Working Group (E. Accomando et al.), *Phys. Rep.* **299** (1998) 1.
- [2] M. Golden, T. Han, G. Valencia, in Electroweak symmetry breaking and new physics at the TeV scale, 292-351, hep-ph/9511206; T.L. Barklow et al., in 1996 DPF/DPB Summer Study on New Directions for High-Energy Physics, Snowmass, CO, 1996, hep-ph/9704217; R. Casalbuoni et al., in Joint ECFA/DESY Study: Physics and Detectors for a Linear Collider, Frascati/London/Muenchen/Hamburg 1996, 289, hep-ph/9708287; R. Casalbuoni et al., e+ e- Linear Collisions 1995, 363, hep-ph/9603297;

- R. Casalbuoni et al., Waikoloa Linear Collid. 1993, 887, hep-ph/9306262; R. Rosenfeld, A.R. Zerwekh, *Phys. Lett.* **B418** (1998) 329; E. Boos et al., *Phys. Rev.* **D57** (1998) 1553; hep-ph/9908409; T. Han, *Int.J.Mod.Phys.* **A13** (1998) 2337; T. Han, in International Workshop Detectors on Linear Colliders, Sitges, Spain, May 1999, hep-ph/9910495.
- [3] R. Casalbuoni, A. Deandrea, S. De Curtis, D. Dominici, R. Gatto, J.F. Gunion, *Nucl. Phys.* **B555** (1999) 3.
- [4] A. Manohar, L. Randall, *Phys. Lett.* **B246** (1990) 537; L. Randall, E.H. Simmons, *Nucl. Phys.* **B380** (1992) 3; V. Lubicz, *Nucl. Phys.* **B404** (1993) 559; R. Casalbuoni, S. De Curtis, D. Dominici, P. Chiappetta, A. Deandrea, R. Gatto, *Z. Phys.* **C65** (1995) 327.
- [5] R. Casalbuoni, S. De Curtis, A. Deandrea, D. Dominici, R. Gatto and J.F. Gunion, hep-ph/9801243, AIP Conference Proceedings 435, Workshop on Physics at the First Muon Collider and at the Front End of a Muon Collider, Eds. S.H. Geer and R. Raja p.772.
- [6] A. B. Bég, H. D. Politzer and P. Ramond, *Phys. Rev. Lett.* **43** (1979) 170; S. Dimopoulos, *Nucl. Phys.* **B168** (1980) 69; J. Ellis, M. K. Gaillard, D. V. Nanopoulos and P. Sikivie, *Nucl. Phys.* **B182** (1981) 529; R.S. Chivukula, M. Golden and E.H. Simmons, *Nucl. Phys.* **B363** (1991) 83.
- [7] S. Dimopoulos, S. Raby and G. L. Kane, *Nucl. Phys.* **B182** (1981) 77.
- [8] E. Eichten, I. Hinchliffe, K. Lane and C. Quigg, *Rev. Mod. Phys.* **56** (1984) 579; E. Eichten, I. Hinchliffe, K. Lane and C. Quigg, *Phys. Rev.* **D34** (1986) 1547.
- [9] R. S. Chivukula, R. Rosenfeld, E. H. Simmons and J. Terning, hep-ph/9503202, in *Electroweak Symmetry Breaking and Beyond the Standard Model*, ed. by T. Barklow, et al. (World Scientific), p. 352.
- [10] V. Lubicz and P. Santorelli, *Nucl. Phys.* **B460** (1996) 3.
- [11] B. King, AIP Conference Proceedings 435, Workshop on Physics at the First Muon Collider and at the Front End of a Muon Collider, Eds. S.H. Geer and R. Raja p.621.
- [12] T. Barklow, private communication, suggests that this might be possible.
- [13] J.F. Gunion and H.E. Haber, *Phys. Rev.* **D48** (1993) 5109.
- [14] D.L. Borden, D.A. Bauer, and D.O. Caldwell, *Phys. Rev.* **D48** (1993) 4018.
- [15] T. Ohgaki *et al.*, *Int. J. Mod. Phys.* **A13** (1998) 2411; *Phys. Rev.* **D56** (1997) 1723.